PROCEEDINGS A

rspa.royalsocietypublishing.org

Research



Cite this article: Muhlestein MB, Goldsberry BM, Norris AN, Haberman MR. 2018 Acoustic scattering from a fluid cylinder with Willis constitutive properties. *Proc. R. Soc. A* **474**: 20180571.

http://dx.doi.org/10.1098/rspa.2018.0571

Received: 21 August 2018 Accepted: 1 November 2018

Subject Areas:

acoustics, wave motion

Keywords:

Willis coupling, metamaterial, fluid, cylinder, scattering

Author for correspondence:

Michael B. Muhlestein

e-mail: Michael.B.Muhlestein@usace.army.mil

Acoustic scattering from a fluid cylinder with Willis constitutive properties

Michael B. Muhlestein¹, Benjamin M. Goldsberry², Andrew N. Norris³ and Michael R. Haberman²

¹U.S. Army Engineer Research and Development Center, 72 Lyme Road, Hanover, NH 03755, USA

²Department of Mechanical Engineering and Applied Research Laboratories, The University of Texas at Austin, 10000 Burnet Road, Austin, TX 78758, USA

³Department of Mechanical and Aerospace Engineering, Rutgers University, Piscataway, NJ 08854, USA

(i) MBM, 0000-0002-4742-0278; ANN, 0000-0001-7577-3698; MRH, 0000-0002-7159-9773

A material that exhibits Willis coupling has constitutive equations that couple the pressurestrain and momentum-velocity relationships. This coupling arises from subwavelength asymmetry and non-locality in heterogeneous media. This paper considers the problem of the scattering of a plane wave by a cylinder exhibiting Willis coupling using both analytical and numerical approaches. First, a perturbation method is used to describe the influence of Willis coupling on the scattered field to a firstorder approximation. A higher order analysis of the scattering based on generalized impedances is then derived. Finally, a finite-element method-based numerical scheme for calculating the scattered field is presented. These three analyses are compared and show strong agreement for low to moderate levels of Willis coupling.

1. Introduction

Recent homogenization research relevant to the topic of metamaterials has noted that acoustical systems with subwavelength asymmetry in properties or structure cannot be adequately described in terms of the standard material properties: mass density and bulk modulus [1–3]. These and other similar systems may be described more appropriately with the Willis constitutive equations, which couple the acoustic pressure and the

momentum density to both the volume strain and the particle velocity using an additional material property called the Willis coupling vector. This additional material property is analogous to bi-anisotropy in electromagnetism [2], and is attractive to designers of acoustic metamaterials as it opens a new dimension of material parameter space relative to standard materials. One potential application of Willis materials, or materials with non-trivial Willis coupling vectors, uses scattering for localization, imaging and classification of objects.

Scattering of mechanical waves from Willis materials has received only limited and tangential attention. Muhlestein & Haberman [4] used a Green's function approach to describe the total displacement field in a Willis elastic matrix with Willis inclusions in the long-wavelength limit, but restricted their analysis to the field immediately surrounding the inclusions. On the other hand, electromagnetic scattering from bi-anisotropic materials has received more attention. Lakhtakia used a Green's function-based approach to describe Rayleigh (long wavelength) scattering from bi-anisotropic ellipsoids within a bi-isotropic background material [5], and described scattering from more general geometries using a discrete-dipole approximation [6]. Jakoby [7] used a propagator matrix formalism to describe scattering of obliquely incident electromagnetic plane waves from impedance cylinders with inhomogeneous bi-anisotropic coatings. Zhang et al. [8] studied the scattering from arbitrary three-dimensional bi-anisotropic materials using a hybrid finite-element-boundary integral method. The problem examined here may be considered as a generalization of previous studies of scalar wave scattering from circular domains in the context of acoustics with anisotropic density [9], anti-plane (SH) elastic waves with anisotropic stiffness [10] and two-dimensional electromagnetics with anisotropic permitivity and permeability [11].

The purpose of this paper is to provide an analytical foundation for scattering of acoustic plane waves from Willis-fluid cylinders. The basic equations of a Willis material are introduced in §2, which also describes the anisotropic wave equation in Willis materials. In §3, an exact analysis of two-dimensional scattering (normal incidence on infinite cylinders) is provided. Since the resulting equations that describe the scattered field do not have analytical solutions, two types of asymptotic expansions for weak Willis coupling are used to provide an explicit description of the scattered field. Section 4 describes a finite-element-based approach to the same problem, which is then compared with and validates the analytical predictions. Some final thoughts are provided in §5.

2. Willis materials

A Willis fluid may be described by the constitutive equations

$$-p = \kappa \varepsilon + \psi \cdot \dot{v} \tag{2.1a}$$

and

$$\mu = \rho \cdot v + \psi \dot{\varepsilon}, \tag{2.1b}$$

where p is the acoustic pressure (hereafter just pressure), ε is the volume strain, v is the particle velocity (hereafter just velocity), μ is the momentum density, κ is the bulk modulus, ρ is the effective mass density tensor and ψ is the Willis coupling vector. For this analysis, the material properties are assumed to be constants with respect to frequency. Note that the standard constitutive equations are recovered if $\psi \to 0$ and $\rho \to \rho I$, where ρ is the standard mass density scalar and I is the second-order identity tensor [12,13]. Assuming a time-harmonic acoustic field ($e^{-i\omega t}$ time convention), the constitutive equations may be inverted to yield

$$\varepsilon = \Delta^{-1} \left[\frac{-p}{\kappa} + \frac{i\omega}{\kappa} \psi \cdot \rho^{-1} \cdot \mu \right], \quad \Delta = 1 + \frac{\omega^2}{\kappa} \psi \cdot \rho^{-1} \cdot \psi$$
 (2.2a)

and

$$v = \Delta^{-1} \cdot \left[\frac{-i\omega}{\kappa} \rho^{-1} \cdot \psi p + \rho^{-1} \cdot \mu \right], \quad \Delta = I + \frac{\omega^2}{\kappa} (\rho^{-1} \cdot \psi) \otimes \psi, \tag{2.2b}$$

where \otimes is the tensor product. For simplicity of this initial analysis, only isotropic mass density tensors will be considered such that $\rho = \rho I$. Then the inverted constitutive equations simplify to

$$\varepsilon = \Delta^{-1} \left[\frac{-p}{\kappa} + \frac{i\omega}{\rho\kappa} \psi \cdot \mu \right], \quad \Delta = 1 + \frac{\omega^2}{\rho\kappa} \psi \cdot \psi$$
 (2.3a)

and

$$v = \Delta^{-1} \cdot \left[\frac{-i\omega}{\rho\kappa} \psi p + \frac{\mu}{\rho} \right], \quad \Delta = I + \frac{\omega^2}{\rho\kappa} \psi \otimes \psi.$$
 (2.3b)

The constitutive equations may be further simplified with the definition of the non-dimensional 'asymmetry factor'

$$W = \frac{\omega \psi}{7} \tag{2.4}$$

and the wavenumber $k = \omega/c$, where $Z = \rho c$ is the characteristic impedance and $c = \sqrt{\kappa/\rho}$ is the wave speed. When combined with the dynamic equation $\dot{\mu} = -\nabla p$, the constitutive equations may then be written as

$$\varepsilon = \frac{-1}{\omega Z} (1 + W^2)^{-1} (kp - W \cdot \nabla p) \tag{2.5a}$$

and

$$v = \frac{-i}{\omega \rho} (I + W \otimes W)^{-1} \cdot (kWp + \nabla p), \tag{2.5b}$$

where $W^2 = W \cdot W$. Note that equation (2.5*b*) may also be written as

$$\mathbf{v} = \frac{-i}{\omega_0} (1 + W^2)(kpW - (W \cdot \nabla p)W + (1 + W^2)\nabla p), \tag{2.6}$$

which may be verified by multiplication by $I + W \otimes W$.

Using the definition of the volume strain rate $\dot{\varepsilon} = \nabla \cdot v$, equations (2.5*a*) and (2.6) may be combined into a single anisotropic wave equation for the acoustic pressure,

$$(1+W^2)\nabla^2 p - (W\cdot\nabla)^2 p + k^2 p = 0. (2.7)$$

In order to see the anisotropy in detail, let $p = p_0 e^{i\xi \cdot x}$, with vector wavenumber $\xi = \xi \hat{n}$ and $|\hat{n}| = 1$. Then equation (2.7) may be written as

$$(1 + W^2 - (W \cdot \hat{n})^2)\xi^2 = k^2.$$
(2.8)

This provides an equation for the phase velocity $c_{\rm ph} = \omega/\xi$ in the \hat{n} direction:

$$c_{\rm ph}^2 = (1 + W^2 - (W \cdot \hat{n})^2)c^2. \tag{2.9}$$

Note that the phase velocity is a minimum and equal to c for $\hat{n}=\pm W/W$, and is a maximum and equal to $c\sqrt{1+W^2}$ in the directions orthogonal to W. The group velocity vector is defined as $c_{\rm gr}={\rm d}\omega/{\rm d}\xi$. It may be evaluated as $c_{\rm gr}=(1/2\omega)({\rm d}c_{\rm ph}^2\xi^2/{\rm d}\xi)$ using equation (2.9) for $c_{\rm ph}^2$, which gives

$$c_{\rm gr} = [(1+W^2)\hat{n} - (W \cdot \hat{n})W]c_{\rm ph}.$$
 (2.10)

As is common in dealing with anisotropic wave equations, it is instructive to consider the inverse of the phase speed, i.e. the slowness $s=1/c_{\rm ph}$. The slowness surface, i.e. the surface $S(x)=s\hat{n}$, therefore, has the form of a prolate spheroid. It may be checked that the direction of the group velocity is perpendicular to the slowness surface, a result that is standard in anisotropic elastic solids [14]. Note that equation (2.10) takes into account the assumption that W is a linear function of ω . If W is independent of ω the group velocity becomes

$$c_{\rm gr0} = \frac{c^2}{c_{\rm ph}} [(1 + W^2)\hat{n} - (W \cdot \hat{n})W]. \tag{2.11}$$

Note that $c_{\rm gr0} \cdot \hat{n} = c_{\rm ph}$, which is typical of frequency-independent anisotropy [14], whereas $c_{\rm gr} \cdot \hat{n} = c_{\rm ph}^3/c^2$. In summary, the dependence of W on ω leaves the direction of $c_{\rm gr}$ unchanged while its magnitude is increased by a factor $c_{\rm ph}^2/c^2 \ge 1$.

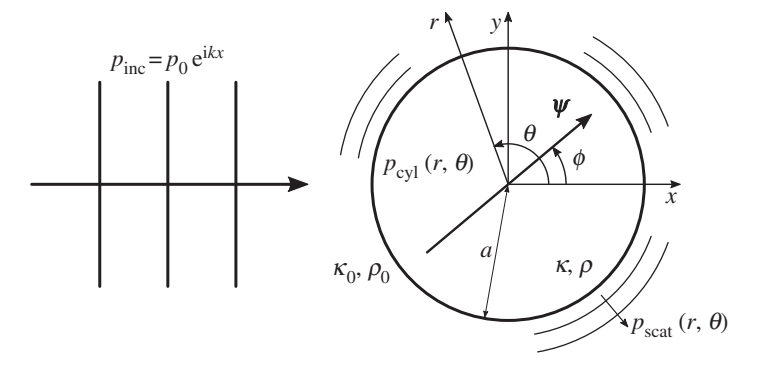


Figure 1. Schematic of plane wave scattering from a Willis-coupled cylinder of radius a. The incident wave has a wavenumber $k_0 = k_0 \hat{x}$. The background material has the mass density ρ_0 and bulk modulus κ_0 and the cylinder has mass density ρ , bulk modulus κ and coupling vector $\boldsymbol{\psi}$.

3. Willis cylinder scattering

Consider a Willis cylinder of radius a, bulk modulus, mass density and Willis coupling vector of κ , ρ and ψ , respectively, in a background fluid with bulk modulus κ_0 , mass density ρ_0 , impedance $Z_0 = \sqrt{\rho_0 \kappa_0}$ and wavenumber $k_0 = \omega \sqrt{\rho_0/\kappa_0}$. Let the origin of a Cartesian coordinate system be set in the centre of the cylinder with the z-axis parallel to the cylinder axis. A schematic of this situation is shown in figure 1. It is worth noting that the cylinder is assumed to have no boundary layer, meaning that the material properties of the cylinder are homogeneous throughout the entire cylinder, including right at the edges. This assumption is equivalent to assuming that the microstructure is sufficiently small compared with a wavelength that interface effects are negligible [15].

Now, consider an incident plane wave propagating in the *x*-direction. The incident wave may be written as

$$p_{\text{inc}} = p_0 e^{ikx} = p_0 \sum_{m=-\infty}^{\infty} i^m J_m(k_0 r) e^{im\theta},$$
 (3.1)

where p_0 is the pressure amplitude and J_m is the mth Bessel function of the first kind. The scattered pressure field may be written as

$$p_{\text{scat}} = p_0 \sum_{m=-\infty}^{\infty} A_m H_m^{(1)}(k_0 r) e^{im\theta},$$
 (3.2)

where $H_m^{(1)}$ is the mth order Hankel function of the first kind. The pressure inside the cylinder satisfies equation (2.7) and can be converted into isotropic form by rescaling the coordinates, which allows the separation of variables solution,

$$p_{\text{cyl}} = \sum_{n} C_n J_n(kR) e^{in\gamma}, \quad \text{where} \quad R = r \sqrt{\frac{1 + W^2 \cos^2(\theta - \phi)}{1 + W^2}},$$

$$\gamma = \tan^{-1} \frac{\tan(\theta - \phi)}{\sqrt{1 + W^2}},$$
(3.3)

and where ϕ denotes the direction of W in terms of the regular polar coordinates r, θ , that is, $W = W\hat{r}(\phi)$, where $\hat{r}(\theta) = r/r$ is the unit vector in the radial direction.

The boundary conditions are continuity of pressure and the normal component of the velocity at the surface of the cylinder. The latter follows from equation (2.5b) as

$$v_r \equiv \boldsymbol{v} \cdot \hat{r} = \frac{-\mathrm{i}}{\alpha \omega} \left(\partial_r p + \frac{\boldsymbol{W} \cdot \hat{r}}{1 + \boldsymbol{W}^2} (kp - \boldsymbol{W} \cdot \nabla p) \right). \tag{3.4}$$

Equations (3.3) and (3.4) provide an exact solution inside the circular cylindrical scatterer of radius a. The difficulty arises in trying to match the interior solution to the exterior one. Specifically, the representation of p in equation (3.3) does not translate to a simple one in terms of r, θ . We, therefore, assume $W \ll 1$ and consider asymptotic expansions of the solution in terms of the small coupling parameter W.

(a) First-order approximation

At this level of approximation, we consider only the contributions of order *W* in the equation for the velocity in equation (2.6) and the pressure in equation (2.7), which become, respectively,

$$\mathbf{v} = -i\frac{W}{Z}p - \frac{\nabla p}{kZ}$$
 and $\nabla^2 p + k^2 p = 0$, (3.5)

where $Z = \sqrt{\rho \kappa}$ is the characteristic impedance of the Willis material. The solution in the cylinder is, therefore,

$$p_{\text{cyl}} = p_0 \sum_{m = -\infty}^{\infty} B_m J_m(kr) e^{im\theta}, \qquad (3.6)$$

where, referring to equation (3.3), $B_m = C_m e^{-im\phi}$. Continuity of the pressure combined with orthogonality yields

$$i^{m}J_{m}(k_{0}a) + A_{m}H_{m}^{(1)}(k_{0}a) = B_{m}J_{m}(ka).$$
(3.7)

The condition for continuity of the normal component of velocity is more complicated to derive (see appendix A), but results in

$$\frac{Z}{Z_0}[i^m J'_m(k_0 a) + A_m H_m^{(1)'}(k_0 a)] = B_m J'_m(k a) + \frac{W}{2}[e^{-i\phi} B_{m-1} J_{m-1}(k a) + e^{i\phi} B_{m+1} J_{m+1}(k a)].$$
(3.8)

Since equation (3.8) depends on B_{m-1} , B_m and B_{m+1} , it becomes impractical to determine A_m and B_m in closed form from equations (3.7) and (3.8). A perturbation analysis, however, may be used to provide explicit expressions up to first order (FO). For $W \ll 1$ but $\neq 0$, the coefficients may be expanded in a series over W as

$$A_m = W^0 A_m^{(0)} + W^1 A_m^{(1)} + W^2 A_m^{(2)} + \cdots$$
(3.9a)

and

$$B_m = W^0 B_m^{(0)} + W^1 B_m^{(1)} + W^2 B_m^{(2)} + \cdots$$
 (3.9b)

Substituting these expansions into equations (3.7) and (3.8) and setting W = 0 (no Willis coupling), the leading coefficients may be written as

$$A_m^{(0)} = -i^m \frac{ZJ_m(ka)J'_m(k_0a) - Z_0J'_m(ka)J_m(k_0a)}{ZJ_m(ka)H_m^{(1)'}(k_0a) - Z_0J'_m(ka)H_m^{(1)}(k_0a)}$$
(3.10a)

and

$$B_m^{(0)} = \frac{2i^{m+1}Z(\pi k_0 a)^{-1}}{ZI_m(ka)H_m^{(1)'}(k_0 a) - Z_0I_m'(ka)H_m^{(1)}(k_0 a)},$$
(3.10b)

which is the classic result of scattering from a fluid cylinder. Substituting from equation (3.9) into equations (3.7) and (3.8), differentiating with respect to W and setting W = 0 yields

$$A_m^{(1)} = \frac{Z_0}{2} \frac{e^{-i\phi} B_{m-1}^{(0)} J_m(ka) J_{m-1}(ka) + e^{i\phi} B_{m+1}^{(0)} J_m(ka) J_{m+1}(ka)}{Z J_m(ka) H_m^{(1)}(koa) - Z_0 J_m'(ka) H_m^{(1)}(koa)}$$
(3.11a)

and

$$B_m^{(1)} = \frac{Z_0}{2} \frac{e^{-i\phi} B_{m-1}^{(0)} H_m(k_0 a) J_{m-1}(k a) + e^{i\phi} B_{m+1}^{(0)} H_m(k_0 a) J_{m+1}(k a)}{Z J_m(k a) H_m^{(1)'}(k_0 a) - Z_0 J_m'(k a) H_m^{(1)}(k_0 a)}.$$
(3.11b)

Combining equations (3.2) and (3.6) with (3.10) and (3.11) gives the FO approximation to the scattered and interior fields,

$$A_m \approx A_m^{(0)} + WA_m^{(1)}, \quad B_m \approx B_m^{(0)} + WB_m^{(1)}.$$
 (3.12)

An important limiting case is that of ka, $k_0a \ll 1$. For mathematical concreteness, let $ka = \eta k_0a$ and assume k_0a is small and η is of order 1. In this case, one finds the $m = 0, \pm 1$ scattering coefficients dominate and may be approximated as

$$A_0 \approx (k_0 a)^2 \frac{\pi}{4} \left[\frac{Z - \eta Z_0}{iZ} + \frac{W \eta Z_0}{Z_0 + \eta Z} 2 \cos(\phi) \right]$$
 (3.13a)

and

$$A_{\pm 1} \approx \pm (k_0 a)^2 \frac{\pi}{4} \left[\frac{Z_0 - \eta Z}{Z_0 + \eta Z} - \frac{iW\eta Z_0}{Z_0 + \eta Z} e^{\mp i\phi} \right].$$
 (3.13b)

Thus in the long-wavelength limit the presence of a uniform Willis coupling modifies the relative strength of the monopole and dipole moments as a function of incidence angle.

(b) Higher order approximation

As shown above, the traditional approach to determining the scattered acoustic fields becomes difficult for higher order (HO) approximations of the pressure equation in equation (2.7). However, a more general approach [16] to acoustic scattering that partitions the solution into three distinct physically meaningful *impedances* reduces the problem to the easier task of finding one of the impedances. As before, assume that the total acoustic pressure p comprises the incident, p_{inc} , and scattered, p_{scat} , components

$$p = p_{\text{inc}} + p_{\text{scat}},\tag{3.14}$$

which for the moment are treated as vectors with an infinite number of components and will later be identified as the coefficients of $e^{im\theta}$. The radial part of the velocity may also be written as infinite vectors as

$$v_r = v_{r,\text{inc}} + v_{r,\text{scat}}. ag{3.15}$$

Surface impedance matrices Z_{inc} , Z_{scat} and Z_{cyl} are then introduced, which are defined such that on the surface bounding the scatterer from the exterior fluid

$$p + Z_{cv1}v_r = 0, (3.16a)$$

$$p_{\rm inc} + Z_{\rm inc} v_{r,\rm inc} = 0 \tag{3.16b}$$

$$p_{\text{scat}} - Z_{\text{scat}} v_{r,\text{scat}} = 0. \tag{3.16c}$$

Assuming that the impedances are known, the solution for the scattered field is just

$$p_{\text{scat}} = Sp_{\text{inc}},\tag{3.17}$$

where the scattering matrix is

and

$$S = (Y_{\text{scat}} + Y_{\text{cyl}})^{-1} (Y_{\text{inc}} - Y_{\text{cyl}}), \tag{3.18}$$

and $Y_{\rm inc}=Z_{\rm inc'}^{-1}$ $Y_{\rm scat}=Z_{\rm scat}^{-1}$ and $Y_{\rm cyl}=Z_{\rm cyl}^{-1}$ are mobility matrices.

In the case considered here the surface is circular, so that the infinite vectors p, v_r , etc. in equation (3.16) represent the components of these physical quantities in terms of $e^{in\theta}$, where θ

is the polar angle and n are integers. We use the standard representation for the incident and scattered pressure,

$$(p_{\text{inc}}, p_{\text{scat}}) = p_0 \sum_{n} (F_n J_n(k_0 r), A_n H_n^{(1)}(k_0 r)) e^{in\theta}$$

$$= p_0 \sum_{n} \left(\hat{F}_n \frac{J_n(k_0 r)}{J_n(k_0 a)}, \hat{A}_n \frac{H_n^{(1)}(k_0 r)}{H_n^{(1)}(k_0 a)} \right) e^{in\theta},$$
(3.19)

where (see equation (3.1)) $F_n = i^n$ for the assumed plane wave incidence. Equation (3.17) then becomes

$$\hat{A} = S\hat{F},\tag{3.20}$$

where \hat{F} and \hat{A} are vectors with elements \hat{F}_n , \hat{A}_n . Alternatively, using the original F and A matrices we may write

$$A = \operatorname{diag}\left(\frac{1}{H_n^{(1)}(k_0 a)}\right) S \operatorname{diag}(J_n(k_0 a)) F, \tag{3.21}$$

where diag(x_n) denotes a diagonal matrix with x_n being the (n, n)th element. Note that Z_{inc} and Z_{scat} (and hence Y_{inc} and Y_{scat}) are diagonal with components

$$[Z_{\rm inc}]_{mn} = -iZ_0 \frac{J_n(k_0 a)}{J'_n(k_0 a)} \delta_{mn}$$
(3.22a)

and

$$[Z_{\text{scat}}]_{mn} = iZ_0 \frac{H_n^{(1)}(k_0 a)}{H_n^{(1)'}(k_0 a)} \delta_{mn}.$$
(3.22b)

The main difficulty is with the impedance or mobility matrices for the cylinder itself. The total fields on the cylinder surface may be represented as

$$(v_r(a), p(a)) = \sum_n (V_n, P_n) e^{in\theta},$$
 (3.23)

and, writing the elements of the cylinder admittance matrix Y_{cyl} as Y_{mn} , the coefficients V_m may be written as

$$V_m = \sum_n Y_{mn} P_n. (3.24)$$

Knowledge of Y_{cyl} is crucial to evaluating the scattered field. Methods for estimating Y_{cyl} are discussed next.

(i) Perturbation solution

A perturbation approach provides a useful means of approximating the true cylinder admittance matrix. First, consider p as a function of polar coordinates such that equation (3.4) becomes

$$v_r = \frac{-i}{\rho\omega(1+W^2)} \left(\left[1 + \frac{W^2}{2} \right] \frac{\partial p}{\partial r} + Wkp\cos(\theta - \phi) - \frac{W^2}{2} \frac{\partial p}{\partial r}\cos 2(\theta - \phi) + \frac{W^2}{2r} \frac{\partial p}{\partial \theta}\sin 2(\theta - \phi) \right). \tag{3.25}$$

Equation (3.25) is relatively simple in r, θ , as compared with the pressure in equation (3.3). This suggests that using the former in an exact sense combined with an approximation for p in equation (3.3) may lead to useful results.

Consider the regime of $W \ll 1$ for which a perturbation solution can be developed. Expanding R and γ of equation (3.3) in the small parameter W gives

$$R = r \left\{ 1 - \frac{W^2}{4} [1 - \cos 2(\theta - \phi)] + O(W^4) \right\}$$

$$\gamma = (\theta - \phi) - \frac{W^2}{4} \sin 2(\theta - \phi) + O(W^4).$$
(3.26)

and

Hence, the pressure and the radial velocity may also be expanded to yield

$$p = \sum_{n} B_{n} e^{in\theta} \left(J_{n}(kr) - \frac{W^{2}}{4} [kr J'_{n}(kr)(1 - \cos 2(\theta - \phi)) + in J_{n}(kr) \sin 2(\theta - \phi)] \right) + O(W^{4}) \quad (3.27a)$$

and

$$v_{r} = \frac{-i}{Z} \sum_{n} B_{n} e^{in\theta} \left(\left(1 - \frac{W^{2}}{2} \right) J'_{n}(kr) + \frac{W^{2}}{4} \left(kr - \frac{n^{2}}{kr} \right) J_{n}(kr) + (W - W^{3}) J_{n}(kr) \cos(\theta - \phi) \right.$$

$$\left. - \frac{W^{2}}{4} \left[\left[2J'_{n}(kr) + \left(kr - \frac{n^{2}}{kr} \right) J_{n}(kr) \right] \cos 2(\theta - \phi) - in \left[\frac{2J_{n}(kr)}{kr} - J'_{n}(kr) \right] \sin 2(\theta - \phi) \right] \right)$$

$$+ O(W^{4}). \tag{3.27b}$$

Equations (3.23) and (3.27) imply that

$$P_m = \sum_n D_{mn} B_n, \quad V_m = \sum_n E_{mn} B_n,$$
 (3.28)

from which the admittance defined in (3.24) is given by

$$Y_{\text{cyl}} = ED^{-1}. (3.29)$$

Recalling that the anisotropic wave equation this analysis is based on is only valid up to $O(W^2)$, only terms up to $O(W^2)$ from equation (3.27) will be retained, which gives the admittance matrices E and D as

$$D_{mn} = \left(J_n(ka) - ka \frac{W^2}{4} J'_n(ka)\right) \delta_{mn} + \frac{W^2}{8} (kaJ'_n(ka) \mp nJ_n(ka)) e^{\mp i2\phi} \delta_{mn\pm 2} + O(W^4)$$
(3.30a)

and

$$E_{mn} = \frac{i}{Z} \left\{ \left(J'_n(ka) + \frac{W^2}{4} \left[\left(ka - \frac{n^2}{ka} \right) J_n(ka) - 2J'_n(ka) \right] \right) \delta_{mn} + \frac{W - W^3}{2} J_n(ka) e^{\mp i\phi} \delta_{mn\pm 1} - \frac{W^2}{8} \left[\left(ka - \frac{n^2}{ka} \right) J_n(ka) + 2J'_n(ka) \mp n \left[\frac{2}{ka} J_n(ka) - J'_n(ka) \right] \right] e^{\mp i2\phi} \delta_{mn\pm 2} \right\} + O(W^4). \quad (3.30b)$$

These expressions may then be used to get a good approximation of the scattering. Note that $\delta_{m\,n+1}$ is a diagonal string of ones below the main diagonal, $\delta_{m\,n-1}$ is above the main diagonal, and the symbols \pm and \mp should be treated as both the plus *and* the minus cases (e.g. $(A\pm B)e^{i\mp c} \equiv (A+B)e^{-ic} + (A-B)e^{ic}$).

(ii) First-order approximation revisited

In order to compare the second-order impedance approach with the FO approximation of $\S 3a$, first write D and E of equations (3.30) as series in W,

$$D = D^{(0)} + W^{2}D^{(2)} + O(W^{4})$$

$$E = E^{(0)} + WE^{(1)} + W^{2}E^{(2)} + O(W^{3}).$$
(3.31)

It then follows from equations (3.29) and (3.30) that to O(W) the impedance is

$$Y_{\text{cyl}} = Y_{\text{cyl}}^{(0)} + WY_{\text{cyl}}^{(1)} + O(W^2), \tag{3.32}$$

where $Y_{\rm cyl}^{(0)}$ is a diagonal matrix and $Y_{\rm cyl}^{(1)}$ is a bi-diagonal matrix

$$Y_{mn}^{(0)} = \frac{1}{Z_n} \delta_{mn} \quad \text{with } Z_n = -iZ \frac{J_n(ka)}{J'_n(ka)}$$
 (3.33a)

and

$$Y_{mn}^{(1)} = \frac{i}{2Z} e^{\mp i\phi} \delta_{mn\pm 1}. \tag{3.33b}$$

Substitution from equation (3.32) into equation (3.18) yields the FO approximation of the scattering matrix,

$$S = S^{(0)} + WS^{(1)} + O(W^2), (3.34)$$

where

$$S^{(0)} = (Y_{\text{scat}} + Y_{\text{cyl}}^{(0)})^{-1}(Y_{\text{inc}} - Y_{\text{cyl}}^{(0)}), \quad S^{(1)} = -(Y_{\text{scat}} + Y_{\text{cyl}}^{(0)})^{-1}Y_{\text{cyl}}^{(1)}(I + S^{(0)}). \tag{3.35}$$

Substituting the two terms from equation (3.34) into (3.21) for plane wave incidence ($F_n = i^n$) it can be shown that $S^{(0)}$ and $S^{(1)}$ produce the analytical expressions for the scattering amplitudes $A_m^{(0)}$ and $A_m^{(1)}$ given by equations (3.10) and (3.11), respectively. The equivalence has also been checked numerically.

(c) Comparison of the first- and higher-order approximations

In order to compare the HO approximation based on equations (3.18), (3.21), (3.29) and (3.30) with the FO approximation of (3.12) we consider how each satisfies the boundary conditions. An exact solution will have perfect continuity of pressure and of radial particle velocity at the boundary r = a. The approximate solutions will display discontinuities of these quantities to differing degrees. Here, we focus on the pressure condition, and define the angle-dependent parameter

$$\Delta p(\theta) = p_{\text{inc}}(a, \theta) + p_{\text{scat}}(a, \theta) - p_{\text{cvl}}(a, \theta). \tag{3.36}$$

Here, p_{inc} and p_{scat} are defined by the incident and scattered fields in equation (3.19). The incident field is assumed to be a plane wave of amplitude p_0 . The internal pressure p_{cyl} is defined by the exact series in equation (3.3) with coefficients determined by equation (3.28). That is, $C_m = e^{\mathrm{i}m\phi} \sum_n (D^{-1})_{mn} P_n$, where P_n are the coefficients of the exterior pressure $p_{\text{inc}}(a) + p_{\text{scat}}(a)$, i.e. $P_n = F_n J_n(k_0 a) + A_n H_n^{(1)}(k_0 a)$, where $F_n = \mathrm{i}^n$ and A_n are determined by the FO or the HO approximation. The matrix D is defined by equation (3.30a) for the HO approximation and is $D_{mn} = J_n(ka)\delta_{mn}$ for the FO approximation. Thus,

$$\Delta p(\theta) = \sum_{n} \{ (F_n J_n(k_0 a) + A_n H_n^{(1)}(k_0 a)) e^{in\theta} - C_n J_n(k R|_{r=a}) e^{in\gamma} \}.$$
 (3.37)

In the following, we present comparisons of the quantity

$$\Delta(\theta) = \left| \frac{\Delta p(\theta)}{p_0} \right|. \tag{3.38}$$

Examples for various values of relevant parameters are shown in figure 2. The parameters in figure 2 cover a wide range of those physically admissible in terms of frequency and impedance. In particular, we note that the HO approximation shows smaller discontinuity in the pressure over a wide range of the perturbation parameter *W*, up to 0.7.

(i) Scattered far field

The comparisons of figure 2 provide confidence that the HO approximation provides more accurate estimates of the scattered pressure for plane wave incidence. Based on this, we show

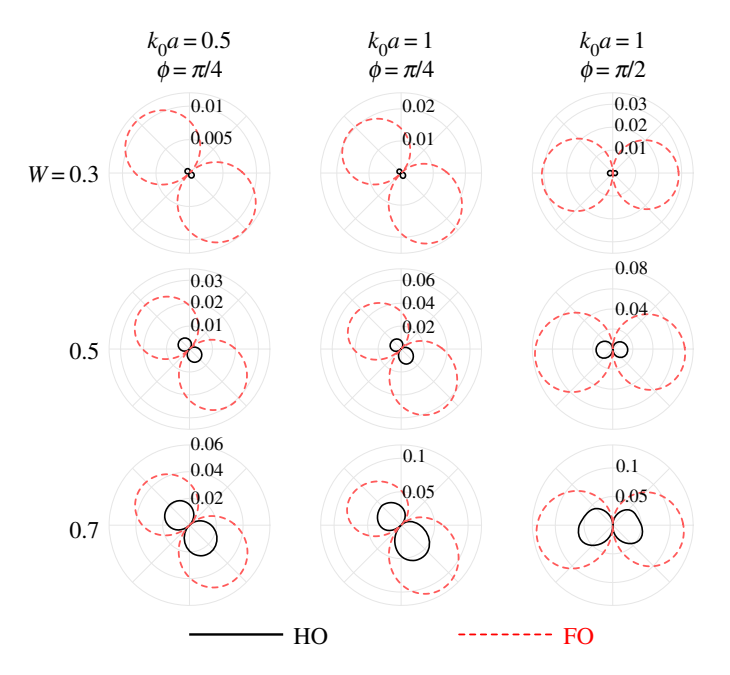


Figure 2. Comparison of the higher order (HO) approximation (solid) and the first-order (FO) approximation (dashed) for values of W from W=0.3 to W=0.7. The polar plots show the values of the pressure boundary condition error $\Delta(\theta)$ of (3.38) for plane wave incidence from the left. Parameters common among all subfigures: $k/k_0=\frac{2}{3}$. (Online version in colour.)

in figure 3 the far-field amplitude for different values of the parameters Z, ϕ , k_0a and for values of W as large as 0.7. These plots indicate that the FO Born approximation is good for values of W less than 0.5. For larger values, the HO approximation indicates different scattering patterns and amplitudes, particularly in some scattering directions.

4. Finite-element analysis

A model based on the finite-element method (FEM) has been derived to assess the accuracy of the approximations in §3. This model provides a solution of the full scattering problem whose error is independent of the magnitude of the Willis coupling vector. Instead, the sources of error are the familiar inaccuracies associated with FEM, including the discretization of the geometry into a triangular mesh and the projection of the scattered field onto a finite set of basis functions. However, the overall error is bounded by the size of the mesh elements, which decreases as the mesh is refined [17].

The geometry of the problem under consideration is shown in figure 1. As with the analytical solutions presented in §3a,b, the FEM will only consider the two-dimensional case since all fields are assumed constant along the z-axis. The resulting far-field calculation of the pressure field will take into account the invariance of the solution along the axis of the cylinder by using the scattered field expansion in equation (3.2). The implementation of FEM requires a variational formulation for the wave equation, often called the weak formulation, which accounts for Willis coupling in the constitutive equations. The derivation of the weak formulation is provided below, followed by the projection of the computed scattered field solution to the far field.

(a) Weak form

Let Ω_W , Ω_F and Γ represent the domains of the Willis fluid, the exterior fluid and the boundary shared between the two domains, respectively (figure 4). The weak form for the acoustic pressure

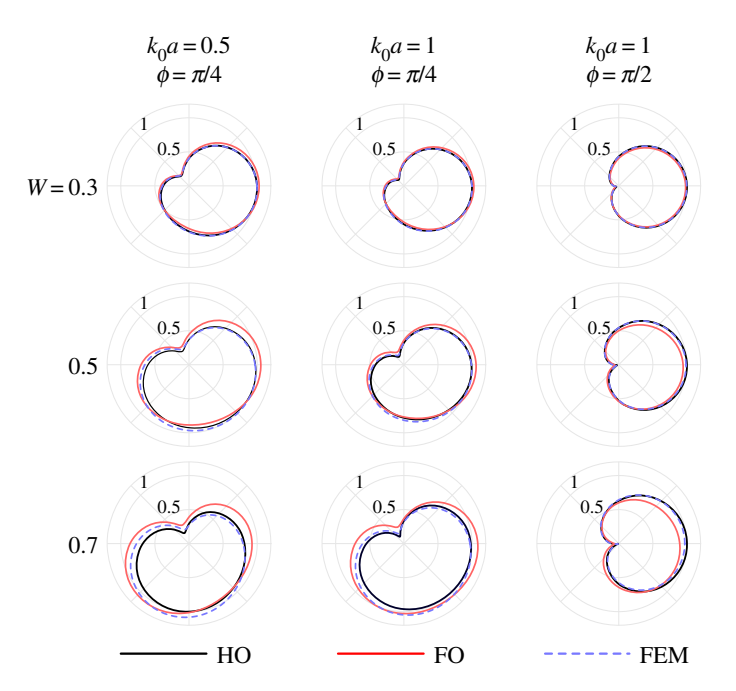


Figure 3. Comparison of the far-field scattering amplitudes using the higher order (HO) approximation and the first order (FO) approximation for plane wave incidence from the left. Predictions using a finite-element method (FEM) that are described in §4 are also shown. Parameters common among all subfigures: $k/k_0 = \frac{2}{3}$.

in the Willis domain is derived by multiplying the time-harmonic equation $\nabla \cdot v + i\omega \varepsilon = 0$ by a test function $\phi_{\rm cyl}$ and integrating over the Willis domain to yield the integral equation

$$\int_{\Omega_W} (\nabla \cdot \mathbf{v}) \phi_{\text{cyl}} \, d\Omega_W + i\omega \int_{\Omega_W} \varepsilon \phi_{\text{cyl}} \, d\Omega_W = 0.$$
 (4.1)

Using Green's identity on the first integral gives the equation

$$-\frac{\mathrm{i}}{\omega} \int_{\Omega_{\mathrm{W}}} \boldsymbol{v} \cdot \nabla \phi_{\mathrm{cyl}} \, \mathrm{d}\Omega_{\mathrm{W}} - \int_{\Omega_{\mathrm{W}}} \varepsilon \phi_{\mathrm{cyl}} \, \mathrm{d}\Omega_{\mathrm{W}} + \frac{\mathrm{i}}{\omega} \int_{\Gamma} \phi_{\mathrm{cyl}}(\boldsymbol{v} \cdot \boldsymbol{n}) \, \mathrm{d}\Gamma = 0, \tag{4.2}$$

where it is assumed that the boundary of the Willis medium completely shares a boundary with the exterior fluid. The relationship for volume strain and velocity fields provided in equations (2.5a)–(2.6) are substituted in equation (4.2) to yield the weak form for the acoustic pressure in a Willis fluid,

$$\begin{split} &\frac{-1}{\omega^{2}\rho(1+W^{2})}\int_{\Omega_{W}}\left[(1+W^{2})\nabla p_{\mathrm{cyl}}\cdot\nabla\phi_{\mathrm{cyl}}-k^{2}p_{\mathrm{cyl}}\phi_{\mathrm{cyl}}+kp_{\mathrm{cyl}}(\boldsymbol{W}\cdot\nabla\phi_{\mathrm{cyl}})+k\phi_{\mathrm{cyl}}(\boldsymbol{W}\cdot\nabla p_{\mathrm{cyl}})\right.\\ &\left.-(\boldsymbol{W}\cdot\nabla p_{\mathrm{cyl}})(\boldsymbol{W}\cdot\nabla\phi_{\mathrm{cyl}})\right]\mathrm{d}\Omega_{\mathrm{W}}+\frac{\mathrm{i}}{\omega}\int_{\Gamma}\phi_{\mathrm{cyl}}(\boldsymbol{v}\cdot\boldsymbol{n})\,\mathrm{d}\Gamma=0. \end{split} \tag{4.3}$$

Similarly, the weak form for the scattered pressure in the exterior fluid, p_{scat} , may be found to be [18]

$$\frac{-1}{\rho_0 \omega^2} \int_{\Omega_{\rm F}} (\nabla p_{\rm scat} \cdot \nabla \phi_{\rm scat} - k_0^2 p_{\rm scat} \phi_{\rm scat}) \, \mathrm{d}\Omega_{\rm F} - \frac{\mathrm{i}}{\omega} \int_{\Gamma} (\boldsymbol{v} \cdot \boldsymbol{n}) \phi_{\rm scat} \, \mathrm{d}\Gamma = \frac{1}{\rho_0 \omega^2} \int_{\Gamma} \phi_{\rm scat} (\nabla p_{\rm inc} \cdot \boldsymbol{n}) \, \mathrm{d}\Gamma,$$
(4.4)

where ϕ_{scat} is the test function of the scattered pressure field in the exterior fluid. Equations (4.3) and (4.4) are combined to yield the total integral equation for the coupled fields (p_{cyl} , p_{scat})

$$\mathcal{I}_{\Omega_{W}} + \mathcal{I}_{\Omega_{E}} = \mathcal{I}_{inc}, \tag{4.5}$$

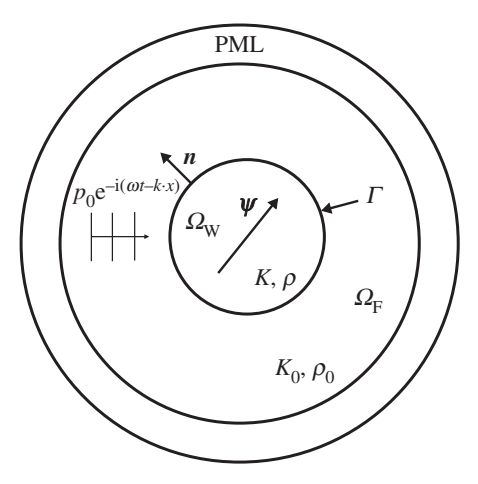


Figure 4. Finite-element method computational domain, where Ω_W is the Willis cylinder, Ω_F is the exterior fluid domain and PML is the perfectly matched layer used to truncate the computational domain.

where $\mathcal{I}_{\Omega_{\mathrm{W}}}$ is the volume integral in equation (4.3), $\mathcal{I}_{\Omega_{\mathrm{F}}}$ is the volume integral in equation (4.4) and $\mathcal{I}_{\mathrm{inc}}$ is the surface integral on the right-hand side of equation (4.4). The surface integrals in equations (4.3) and (4.4) are used to describe the continuity of normal particle velocity at the interface, as described below. Galerkin's method is used to numerically solve equation (4.5) by seeking approximations to p_{cyl} and p_{scat} that are written as a linear combination of basis functions, which are chosen to be piecewise quadratic Lagrange polynomials [19]. The continuity of pressure on the interface, $p_{\mathrm{cyl}} = p_{\mathrm{inc}} + p_{\mathrm{scat}}$, is directly enforced on the basis functions. The weak form is made symmetric by choosing test functions that are represented with the same basis functions as the unknown dependent variables. Given this choice in test functions supplemented with the fact that the incident wave is known, the continuity of normal particle velocity is naturally enforced

$$\frac{\mathrm{i}}{\omega} \int_{\Gamma} \phi_{\text{cyl}}(\mathbf{v} \cdot \mathbf{n}) \, \mathrm{d}\Gamma - \frac{\mathrm{i}}{\omega} \int_{\Gamma} \phi_{\text{scat}}(\mathbf{v} \cdot \mathbf{n}) \, \mathrm{d}\Gamma = 0, \tag{4.6}$$

and therefore does not appear in equation (4.5). Equation (4.5) is solved using the finite-element software package COMSOL Multiphysics using the weak form PDE module and making use of built-in perfectly matched layers to truncate the computational domain (figure 4) and satisfy the Sommerfeld radiation condition [18,20]. A sufficiently fine mesh of the computational domain was used to obtain convergence. It is also worthwhile noting that the exterior fluid can be modelled with a boundary integral method instead of equation (4.4). A hybrid FEM/boundary-element method may be obtained using similar techniques in acoustic fluid–structure interaction problems [21].

(b) Far-field calculation

The far-field solution is found by numerically calculating the scattered field coefficients in equation (3.2), which can then be compared with the approximate solutions found using the methods developed in §3. The resulting p_{scat} from the FEM at a radius b is expanded into outward-propagating cylindrical waves

$$p_{\text{scat}}(r=b,\theta) = \sum_{-\infty}^{\infty} A_m H_m^{(1)}(k_0 b) e^{im\theta},$$
 (4.7)

where *b* is chosen to be a sufficient distance away from the cylinder surface such that the evanescent waves are attenuated. Numerical studies show that a radius of one wavelength from

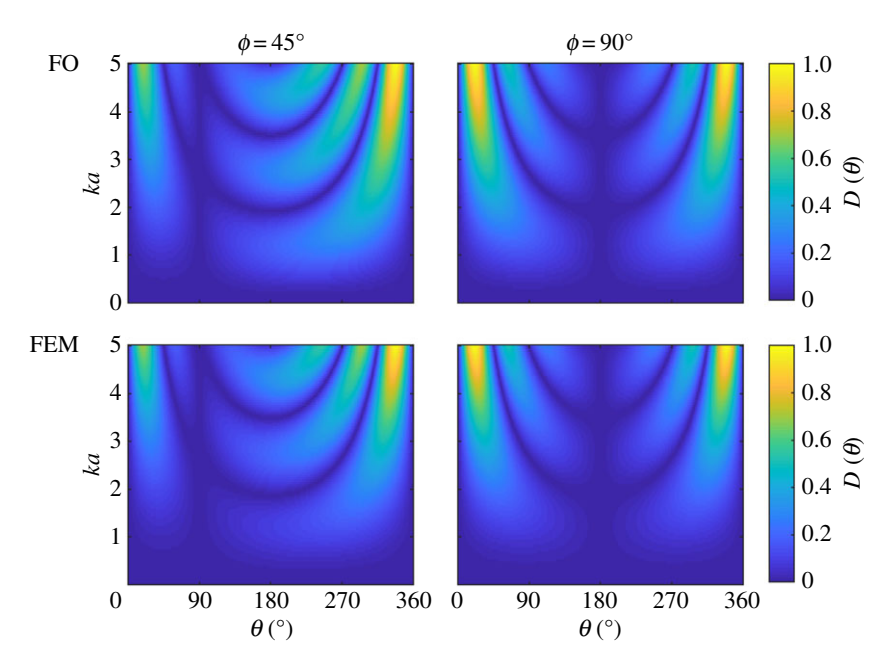


Figure 5. Scattered directivity of a plane wave incident upon a Willis-coupled cylinder. The directivity is shown as a function of the wavenumber multiplied by the cylinder radius ka and of the scattered angle θ . Directivities are shown using the first-order (FO) approximation and a finite-element method (FEM) and for $\phi=45^\circ$ and $\phi=90^\circ$, where ϕ represents the orientation of the Willis coupling vector.

the cylinder surface is sufficient. Orthogonality in θ is used to uniquely determine the scattered field coefficients using a Fourier integral

$$A_m = \frac{1}{2\pi H_m^{(1)}(k_0 b)} \int_{-\pi}^{\pi} p_{\text{scat}}(r = b, \theta) e^{-im\theta} d\theta.$$
 (4.8)

The above integral is a Fourier transform, which may be numerically approximated using optimized algorithms such as the fast Fourier transform.

The directivity pattern for the FEM prediction is shown in figure 3 along with the analytical predictions. As may be seen in figure 3, the FEM and analytical predictions are nearly identical for W = 0.3, and the behaviour of each prediction is qualitatively the same for all cases shown. As W increases the FEM prediction is consistently closer to the HO prediction than to the FO prediction. The similarity of the HO and FEM predictions despite their different approaches suggests that the results are accurate.

Plots of the directivity patterns of the FO and FEM predictions as a function of ka and θ are shown in figure 5 for $\phi=45^\circ$ and $\phi=90^\circ$. For these plots W=0.1 and $k_0a=ka$. As may be seen in the figure, there is no discernible difference between the FO and FEM predictions, suggesting that the FO approximation is sufficient to provide accurate predictions for these conditions.

5. Conclusion

Two types of approximations have been derived for small values of the non-dimensional Willis coupling W. Numerical results compare the FO O(W) and HO O(W³) approximations in terms of how well they satisfy the pressure boundary condition. As expected the HO approximation shows less error. Comparisons of the scattered far fields indicate that the O(W) approximation does not differ much from the O(W³) approximation for $W \le 0.7$. This suggests that the simpler FO approximation may as well be used, especially for smaller values of W.

Furthermore, a FEM for predicting the far-field scattering pattern that is not limited to small W or cylindrical geometry of the scatterer has been developed and implemented. This additional method was compared with the FO and HO analytical approximations and good agreement was found for $W \leq 0.7$. The correlation of the numerical and analytical predictions provides support for both solutions and suggests that Willis coupling does indeed modify the far-field scattering pattern in measurable ways.

Data accessibility. No data have been generated associated with this paper.

Authors' contributions. M.B.M. derived the first-order approximation and A.N.N. derived the higher order approximation. B.M.G. developed and implemented the finite-element analysis. M.R.H. provided valuable insight, which guided the derivations given. All authors gave final approval for publication.

Competing interests. We declare we have no competing interests.

Funding. This work was supported in part by ONR through MURI grant no. N00014-13-1-0631 and YIP grant no. N0014-18-1-2335, and in part by the U.S. Army Engineer Research and Development Center (ERDC), Geospatial Research and Engineering business area. Permission to publish was granted by the Director, Cold Regions Research and Engineering Laboratory.

Acknowledgements. The work for this paper was performed independently by the authors.

Appendix A. First-order particle velocity boundary condition

The FO approximation to the normal component of the incident, scattered and interior particle velocities at the surface of the cylinder are given by

$$\hat{r} \cdot \mathbf{v}_{\text{inc}}|_{a} = -\frac{1}{k_0 Z_0} \frac{\partial p_{\text{inc}}}{\partial r} \bigg|_{r=a} = \frac{-p_0}{Z_0} \sum_{m=-\infty}^{\infty} \mathbf{i}^m J'_m(k_0 a) \, e^{\mathbf{i}m\theta}, \tag{A 1}$$

$$\hat{r} \cdot \mathbf{v}_{\text{scat}}|_{a} = -\frac{1}{k_{0}Z_{0}} \frac{\partial p_{\text{scat}}}{\partial r} \bigg|_{r=a} = \frac{-p_{0}}{Z_{0}} \sum_{m=-\infty}^{\infty} A_{m} H_{m}^{(1)'}(k_{0}a) e^{im\theta}$$
(A 2)

and

$$\hat{r} \cdot \mathbf{v}_{\text{cyl}}|_{a} = -\frac{1}{kZ} \frac{\partial p_{\text{cyl}}}{\partial r} \Big|_{r=a} - i \frac{\hat{r} \cdot \mathbf{W}}{Z} p_{\text{cyl}} \Big|_{r=a}$$

$$= -\frac{p_{0}}{Z} \sum_{m=1}^{\infty} \left[B_{m} J'_{m}(ka) + i \hat{r} \cdot \mathbf{W} B_{m} J_{m}(ka) \right] e^{im\theta}. \tag{A 3}$$

In order to apply orthogonality, all of the θ dependence should be represented by the $e^{im\theta}$ term, which is not the case in the form due to the presence of \hat{r} . Note that

$$\hat{r} \cdot W = W \cos(\theta - \phi) = \frac{W}{2} [e^{i\theta} e^{-i\phi} + e^{-i\theta} e^{i\phi}]. \tag{A4}$$

Then we may write

$$\sum_{m=-\infty}^{\infty} \hat{r} \cdot W B_m J_m(ka) e^{im\theta} = \frac{W}{2} \sum_{m=-\infty}^{\infty} [e^{i\theta} e^{-i\phi} + e^{-i\theta} e^{i\phi}] B_m J_m(ka) e^{im\theta}$$
(A 5)

$$= \frac{W}{2} \sum_{m=-\infty}^{\infty} [e^{-i\phi} B_{m-1} J_{m-1}(ka) + e^{i\phi} B_{m+1} J_{m+1}(ka)] e^{im\theta}.$$
 (A 6)

Now, applying orthogonality results in the condition (3.8).

References

- 1. Alù A. 2011 First-principles homogenization theory for periodic metamaterials. *Phys. Rev. B* **84**, 075153. (doi:10.1103/PhysRevB.84.075153)
- 2. Sieck CF, Alù A, Haberman MR. 2015 Dynamic homogenization of acoustic metamaterials with coupled field response. *Phys. Procedia* **70**, 275–278. (doi:10.1016/j.phpro.2015.08.153)
- 3. Muhlestein MB, Sieck CF, Alù A, Haberman MR. 2016 Reciprocity, passivity and causality in Willis materials. *Proc. R. Soc. A* **472**, 20160604. (doi:10.1098/rspa.2016.0604)

- 4. Muhlestein MB, Haberman MR. 2016 A micromechanical approach for homogenization of elastic metamaterials with dynamic microstructure. *Proc. R. Soc. A* **472**, 20160438. (doi:10.1098/rspa.2016.0438)
- 5. Lakhtakia A. 1991 Rayleigh scattering by a bianisotropic ellipsoid in a biisotropic medium. *Int. J. Electron.* **71**, 1057–1062. (doi:10.1080/00207219108925546)
- 6. Lakhtakia A, Weiglhofer WS. 1992 Scattering by an electrically small bianisotropic sphere in a gyroelectromagnetic uniaxial medium. *Antennas Propag. IEEE Proc. H Microw.* **139**, 217–220. (doi:10.1049/jp-h-2.1992.0040)
- 7. Jakoby B. 1997 Scattering of obliquely incident waves by an impedance cylinder with inhomogeneous bianisotropic coating. *IEEE Trans. Antennas Propag.* **45**, 648–655. (doi:10.1109/8.564091)
- 8. Zhang Y, Wei X, Li E. 2004 Electromagnetic scattering from three-dimensional bianisotropic objects using hybrid finite element-boundary integral method. *J. Electromagn. Waves Appl.* **18**, 1549–1563. (doi:10.1163/1569393042954857)
- 9. Torrent D, Sánchez-Dehesa J. 2009 Sound scattering by anisotropic metafluids based on two-dimensional sonic crystals. *Phys. Rev. B* **79**, 174104. (doi:10.1103/PhysRevB.79.174104)
- 10. Boström A. 2015 Scattering by an anisotropic circle. Wave Motion 57, 239–244. (doi:10.1016/j.wavemoti.2015.04.007)
- 11. Wu XB, Ren W. 1995 Wave-function solution of plane-wave scattering by an anisotropic circular cylinder. *Microw. Opt. Technol. Lett.* **8**, 39–42. (doi:10.1002/mop.4650080114)
- 12. Willis JR. 1981 Variational principles for dynamic problems for inhomogeneous elastic media. *Wave Motion* **3**, 1–11. (doi:10.1016/0165-2125(81)90008-1)
- 13. Willis JR. 1997 Dynamics of composites. In *Continuum micromechanics* (ed. P Suquet), pp. 265–290. International Centre for Mechanical Sciences. Vienna, Austria: Springer.
- 14. Musgrave MJP. 2003 Crystal acoustics. New York, NY: Acoustical Society of America.
- 15. Srivastava A, Willis JR. 2017 Evanescent wave boundary layers in metamaterials and sidestepping them through a variational approach. *Proc. R. Soc. A* **473**, 20160765. (doi:10.1098/rspa.2016.0765)
- 16. Bobrovnitskiĭ YI. 2006 Impedance theory of sound scattering: general relations. *Acoust. Phys.* **52**, 513–517. (doi:10.1134/S1063771006050034)
- 17. Gockenbach MS. 2006 *Understanding and implementing the finite element method*. Philadelphia, PA: SIAM.
- 18. Ihlenburg F. 2006 *Finite element analysis of acoustic scattering*. Berlin, Germany: Springer Science & Business Media.
- 19. Reddy JN. 1993 An introduction to the finite element method, vol. 2. New York, NY: McGraw-Hill.
- 20. COMSOL, Inc. 2017 Acoustics Module User Guide, version 5.3a. http://www.comsol.com.
- 21. Demkowicz L, Oden JT. 1996 Application of Hp-adaptive BE/FE methods to elastic scattering. *Comput. Methods Appl. Mech. Eng.* 133, 287–317. (doi:10.1016/0045-7825(95)00945-0)